

DERIVATION OF THE THERMAL CONDUCTIVITY IN A LATENT THERMAL ENERGY STORAGE UNIT FOR USE IN SIMPLIFIED SYSTEM MODELS

Lauritz Zendel^{1*}, Chiara Springer¹, Frank Dammel¹, Peter Stephan¹

¹Institute for Technical Thermodynamics, Technical University of Darmstadt, Darmstadt, Germany

*Corresponding Author: zendel@ttd.tu-darmstadt.de

ABSTRACT

Latent Thermal Energy Storages (LTES) can store thermal energy in a narrow temperature range. Therefore, they are favorable for integration into Rankine-based Carnot Batteries, heat pumps and heat engines. For the design and optimization of such systems, numerical simulations based on accurate system models are highly desirable. However, physical phenomena such as natural convection in LTES units cannot be modeled directly in transient system models. Simplified models are required. Therefore, the objective of this work is to derive simplified LTES unit models for use in system models.

While an LTES is usually modeled with a fixed temperature level in stationary simulations, in transient simulations the state of charge of the LTES influences its temperature profile. The temperature profile in turn depends on the geometry of the LTES unit. Therefore, the geometry must be taken into account in order to model the transient behavior of an LTES unit with sufficient accuracy.

The LTES unit under investigation has a shell and tube heat exchanger structure, using hexagonal finned tubes. The phase change material (PCM), which stores thermal energy by changing phase from solid to liquid, is located between the fins and in the space between the finned tubes. Aluminum fins are used. They have a high thermal conductivity and thus compensate for the low thermal conductivity of the sodium nitrate used as the PCM. The interaction between the fins and the PCM is complex and cannot be described analytically.

Therefore, a numerical approach can be used to gain insight into the behavior of the LTES unit. In order to transfer the results of a complex numerical model to a simplified model where fins and PCM are not considered individually, the effective thermal conductivity of a single finned tube can be used to approximate the performance of the LTES unit.

In this study, a finite element model of a section with a single finned tube is developed using the COMSOL Multiphysics software. The effective thermal conductivity of the system is determined by varying the effective thermal conductivity of both the liquid and the solid PCM in a simplified model and comparing the resulting average temperature and heat flow curves with reference cases based on a more complex modeling approach. The results can serve as model input for simplified system models of heat pumps, heat engines or Carnot Batteries, among others.

1 INTRODUCTION

Energy storage can play an important role in energy systems. Thermal energy storage can be used, for example, for waste heat recovery (van der Hoeven, 2014), in buildings, in district heating networks, in power generation and in heat exchangers (Ali et al., 2024). In contrast to the already well-developed sensible thermal energy storage systems, Latent Thermal Energy Storage (LTES) systems can have a higher energy density and enable efficient operation due to their narrow temperature range (Steinmann, 2022). There are different types of LTES. Active systems, encapsulation and extending the heat transfer surface are some of the possible designs (Steinmann, 2022). The latter can be further divided into longitudinal and annular finned shell-and-tube heat exchangers (Steinmann, 2022), as illustrated in Figure 1.

The influence of longitudinal fins was investigated by Kirincic et al., 2024. A distinction was made between charging, discharging and a combination of both processes. Two optimizations were carried out. In one, the average latent heat flow and in the other, the thermal effectiveness of the LTES unit was used as the target value. As part of the optimization, the maximum permissible aspect ratio was selected for both target values, while the thickness and number of fins took on an optimum value between the upper and lower limits. Thereby, a potential for improvement compared to an existing LTES unit could be demonstrated.

A comparison of longitudinal and annular fins was carried out by Tiari and Hockins, 2021. With the same fin volume, two longitudinal and two annular fin arrangements were experimentally compared with a configuration

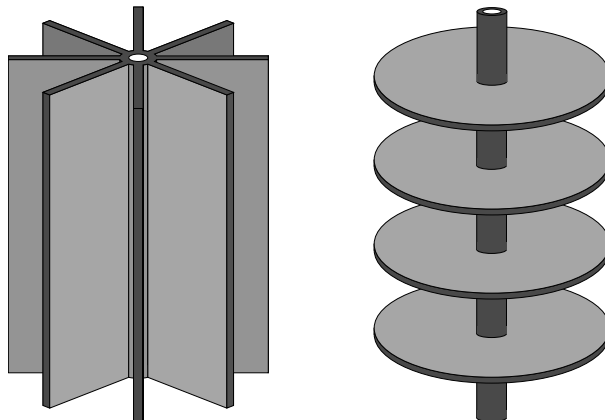


Figure 1: LTES with longitudinal fins (left) and annular fins (right)

without fins in terms of their effects on the charging and discharging duration. It was shown that a higher number of fins, which were thinner due to the restriction of the same volume, enabled a higher thermal power and thus lower charging and discharging durations. The lowest durations were achieved with the configuration with the thin longitudinal fins.

Tiari et al., 2021, also investigated annular fins numerically, maintaining the requirement that the fin volume of each configuration must be identical. In addition to a constant fin length, configurations with linearly increasing and decreasing fin lengths in the axial storage direction were also investigated. It turned out that in terms of the duration for a charging and subsequent discharging cycle, the best results can be achieved with the configurations that have a constant fin length. Again, the configuration with thinner fins is better than the one with fewer thicker ones. If only the charging process is considered, the configurations in which the fins at the lower end of the LTES unit have a larger radius are superior, as they favor the positive influence of natural convection. This shows that natural convection can certainly have a relevant influence.

Nevertheless, natural convection is usually neglected in modeling in order to reduce the computational effort (Steinmann, 2022). While this effect has a negligible influence during solidification, it increases heat transfer during the melting process (Steinmann, 2022).

The study by Vogel and Johnson, 2019, focuses on the influence of natural convection on heat transfer during the charging of an LTES unit. Three branched axial configurations and one with annular fins were investigated numerically. With Ansys Fluent, 3D simulations were carried out, in order to evaluate the temporal progressions of the heat flux and the liquid phase fraction. A convective enhancement factor, which is the ratio of the heat flux taking into account natural convection to the heat flux without it, is plotted and evaluated over the liquid phase fraction. The convective enhancement factors initially increase with increasing liquid phase fraction and, depending on the configuration, show a maximum at different liquid phase fractions, which is above 60 % in all cases investigated, often even close to or above 90 %. For the geometry with annular fins, a maximum convective enhancement factor of 1.6 is achieved, although the value is significantly lower over a wide range of the liquid phase fraction. With longitudinal fins, the maximum value ranges from 1.1 to 4.7 and thus varies significantly depending on the configuration investigated.

The study by Román et al., 2024, is also aimed at possible model simplifications. The LTES unit under investigation consists of several rectangular slabs filled with PCM, with air gaps between them. The influence of the thermal conductivity of the PCM and the possibility of a simplified modeling of the temperature-dependent phase change enthalpy are examined. The thermal conductivity has a small effect on the two investigated quantities, the heat flux and the outlet temperature of the heat transfer fluid air, provided that the thermal resistance due to the heat transfer from the heat transfer fluid to the pipe wall dominates the thermal resistance due to heat conduction in the PCM. The assumption of a different heat transfer fluid (HTF), a constant heat flux or a constant wall temperature could therefore significantly change the results, as the thermal resistance of HTF to the pipe is significantly reduced or completely eliminated. The interrelation between the heat transfer coefficient of the HTF to the pipe and the relevance of the thermal conductivity of the PCM is also assumed by Tehrani et al., 2016. As far as the temperature-dependent phase change enthalpy is concerned, it turned out that a linear relationship in the phase change interval may be sufficient (Román et al., 2024).

In the case of shell and tube heat exchangers, the approach of considering fins and PCM together is also pursued.

For example Parry et al., 2014, scale the effective thermal conductivity of the PCM in a 1D model in order to obtain the results of a 3D model. The associated parameter is selected depending on the existing geometry and thus depending on whether and which fins are present. In the study by Waser et al., 2018, an analytical calculation of the effective thermal conductivity is carried out, which results from a parallel arrangement of PCM and fins. PCM and fins are weighted according to their volume fraction. The thermal conductivity obtained in this way is compared with that from a calibration, whereby similar results are achieved using the 1D model applied.

In contrast to the assumption of an exclusively parallel arrangement of PCM and fins for calculating the effective thermal conductivity, some studies introduce factors that weight the effective thermal conductivity of a parallel and a serial arrangement. Tay et al., 2014, derived an empirical equation using a numerical model to determine a factor that weights the thermal resistances of a parallel and serial arrangement, whereby only thermal conduction is taken into account for the calculation. The factor varies greatly depending on the fins used per meter and the thermal conductivity of the PCM employed. Based on transient simulations, the study by Dietrich, 2017, determines a factor of 0.45 for the weighting of the thermal conductivity of the parallel arrangement as the factor that provides the best agreement between simulation results and experimental data. For annular fins, Vogel et al., 2020, determined a factor of 0.8 for the weighting of the parallel arrangement, whereas a factor of 0.7 was determined for longitudinal fins.

It becomes clear that the factors determined, although they are not defined identically and therefore deviations between the values are to be expected, differ considerably from one another. In this study, the effective thermal conductivity of an annular finned tube with PCM between the fins is therefore examined using a detailed COMSOL model. The effective thermal conductivity of PCM with fins is determined for both the liquid and the solid phase of the PCM, which best approximates a detailed model that serves as a reference case. The results obtained in this way can be used for system simulations and complement previous studies aimed at estimating the effective thermal conductivity.

2 MODELING

The modeling is carried out with the software COMSOL Multiphysics Version 6.2. A 2D axisymmetric computational domain is assumed. Structured rectangular grids with linear shape functions for the temperature, the velocity components and the pressure field are applied.

2.1 Modeled section and material properties

The LTES unit under investigation has the geometry of a vertical shell-and-tube heat exchanger. Each individual tube has hexagonal fins. In this study, a representative section of such a tube is modeled in order to approximate the overall behavior of the LTES unit. For this purpose, the hexagonal fins are modeled as annular fins. Figure 2 shows a section of the LTES unit examined and the modeled representative section.

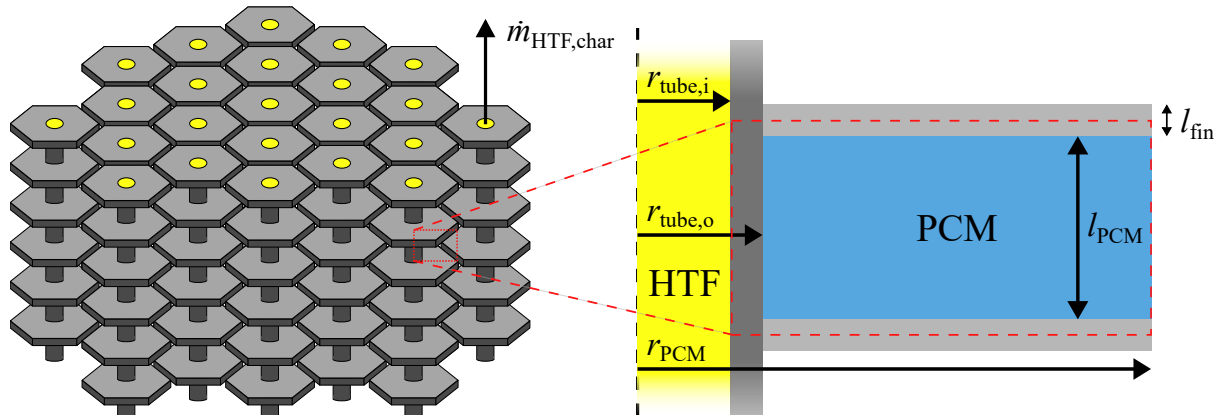


Figure 2: Section of the LTES unit and detailed view, with the modeled representative section highlighted by a red dashed line. The modeled representative section is assumed to be annular

The tube in which the HTF flows is made of steel, the fins of aluminum and sodium nitrate (NaNO_3) is chosen as PCM. The dimensions of the tube are given in Table 1 and are derived from the dimensions of the laboratory test rig by Laing et al., 2009, given in Dietrich, 2017. The experimental data from Laing et al., 2010, are used for

validation. Similar dimensions were also used for a 680 kWh prototype that was installed in Spain (Laing et al., 2010). The material properties are listed in Table 2, which also contains the data of the HTF Therminol VP-1 used in the validation and backtesting case. If necessary, the material properties were interpolated to a temperature of 306 °C.

Table 1: Finned tube dimensions in mm

$r_{\text{tube},i}$	$r_{\text{tube},o}$	r_{PCM}	l_{PCM}	l_{fin}
5	6	50	10	1

To avoid mass changes of NaNO_3 in the calculation area, the average value of $\rho_{\text{NaNO}_3,\text{av}} = 2014 \text{ kg m}^{-3}$ from the density of the liquid phase of $\rho_{\text{NaNO}_3,\text{l}} = 1908 \text{ kg m}^{-3}$ (Bauer et al., 2012) and the solid phase of $\rho_{\text{NaNO}_3,\text{s}} = 2120 \text{ kg m}^{-3}$ (Dietrich, 2017) was used in both phases. Temperature-independent values were assumed for the thermal conductivity and dynamic viscosity in the solid phase. The following temperature-dependent thermal conductivity from Nagasaka and Nagashima, 1991, was assumed for the liquid PCM:

$$\lambda_{\text{NaNO}_3,\text{l}} = \left(0.6203 - 1.8 \times 10^{-4} \cdot \frac{T}{\text{K}} \right) \text{ W m}^{-1} \text{ K}^{-1} \quad (1)$$

The temperature-dependent dynamic viscosity is taken from Nunes et al., 2006, where $\eta_{\text{base}} = 3.033 \text{ mPa s}$ is to be used:

$$\eta_{\text{NaNO}_3,\text{l}} = \eta_{\text{base}} \cdot e^{\left(26.689 - \frac{97.54}{580\text{K}} + \frac{112.5}{(580\text{K})^2} - \frac{41.7}{(580\text{K})^3} \right)} \text{ kg m}^{-1} \text{ s}^{-1} \quad (2)$$

Table 2: Material properties with data taken or linearly interpolated [i] to the temperature 306 °C from Ullrich and Bodmer, 2019, Dietrich, 2017, Bauer et al., 2012, Jriri et al., 1995, Janz, 1967, and Eastman Chemical Company, 2022

Property	Steel	Aluminum	NaNO_3	Therminol VP-1
ρ in kg m^{-3}	7980	2710	2014	810.4 [i]
c in $\text{J kg}^{-1} \text{ K}^{-1}$	531.8 [i]	1034.88 [i]	1658	2330.2 [i]
λ in $\text{W m}^{-1} \text{ K}^{-1}$	18.12 [i]	231.64 [i]	Eq. 1 / 0.7	0.0953 [i]
η in $\text{kg m}^{-1} \text{ s}^{-1}$	-	-	$\text{Eq. 2} / \eta_{\text{base}} \times 10^6$	2.15×10^{-4} [i]
t_{PC} in °C	-	-	306	-
ΔT_{PC} in K	-	-	5	-
h_{PC} in kJ kg^{-1}	-	-	178	-
β in K^{-1}	-	-	7.15×10^{-4}	-

Four different models are used for the study. These are shown in Figure 3 and are described in the following.

2.2 Validation model

The model for the validation case is shown in Figure 3a. Convective heat transfer is present on the inside of the tube carrying the HTF. The input and the output temperature of the HTF as well as the average PCM temperature were visually reconstructed using the online tool WebPlotDigitizer (Rohatgi, 2023). While the experimental average temperature of the HTF is specified in the model the experimental average PCM temperature serves as validation value. A flow velocity $v_{\text{HTF}} = 1.97 \text{ m s}^{-1}$ was selected according to the data from Laing et al., 2009. The correlations of Gnielinski, 2019, were used to calculate the Nusselt number, assuming a fully developed turbulent pipe flow. A heat transfer coefficient $\alpha = 4060.3 \text{ W m}^{-2} \text{ K}^{-1}$ was calculated in this way.

A heat loss flow is given on the outside of the pipe containing the PCM. The value $\dot{Q}_{\text{loss}} = 0.4931 \text{ W}$, which is based on the losses reported in Laing et al., 2009, and the ratio of the section considered for modeling compared

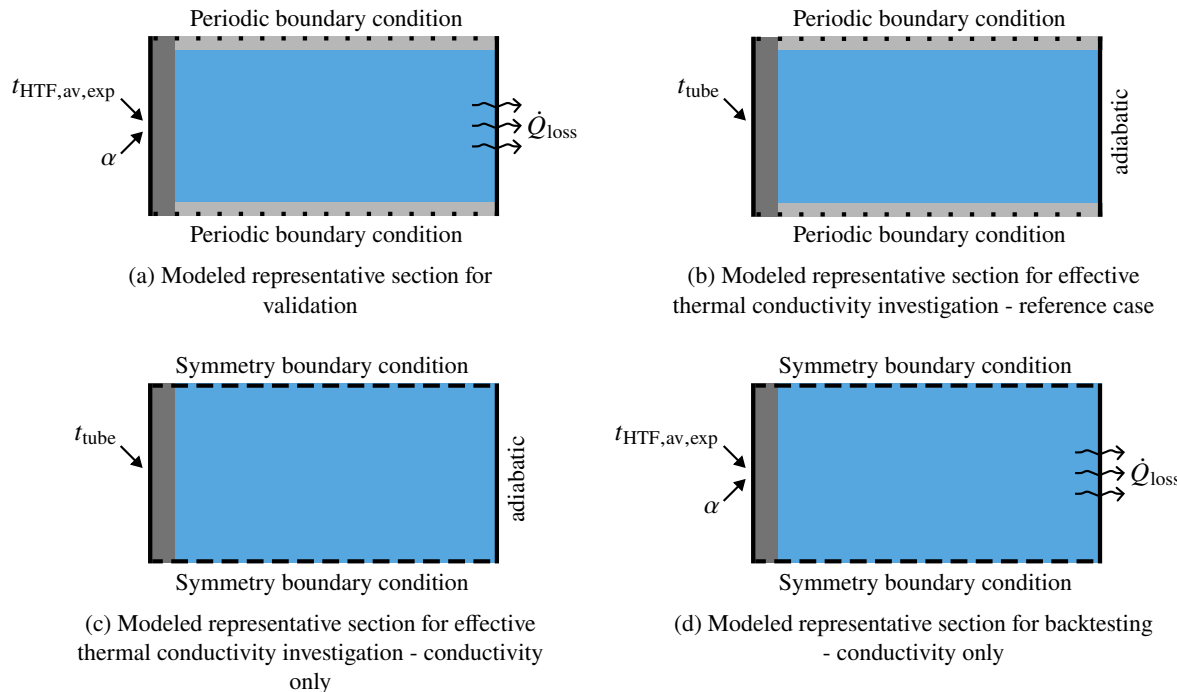


Figure 3: Modeled representative section for validation (a), for effective thermal conductivity investigation - reference case (b), for effective thermal conductivity investigation - conductivity only (c) and for backtesting - conductivity only (d).

to the total length of all storage pipes, is specified. Detailed modeling is not required for transfer to a real storage tank, as the heat losses can be neglected if the real tank is sufficiently large.

Periodic boundary conditions are assumed for the top and bottom of the calculation area.

In COMSOL Multiphysics, the Heat Transfer in Solids and Fluids Interface and the Laminar Flow Interface are coupled with each other using Nonisothermal Flow. In this way, both the heat conduction in the entire calculation area and the flow of the PCM, which is assumed to be an incompressible Newtonian fluid for which conservation of mass, momentum and energy apply (COMSOL AB, 2024), can be modeled. This enables the modeling of natural convection. The underlying equations can be found in the documentation (COMSOL AB, 2024).

A phase change material is added as a liquid for modeling the PCM. This contains the method of apparent heat capacity. The phase change temperature, the phase change interval and the phase change enthalpy must be specified, which can be found in Table 2. The resulting apparent specific heat capacity as a function of temperature, the distribution of the phase change enthalpy and the temperature interval of this distribution can be seen in Figure 4. The coefficient of thermal expansion is utilized to take natural convection into account. Since the density is specified as constant, but a volume force dependent on the temperature is defined, the Boussinesq approximation is applied in this way.

2.3 Reference case model

The reference case model is shown in Figure 3b. The first step for further investigations is to define reference cases so that studies can be carried out independently of the validation case. The model from the validation is modified in such a way that a temperature is specified instead of the temperature of the HTF and a heat transfer coefficient. In addition, the losses are set to zero, in accordance with the fact that heat losses become negligible with large storage capacities.

2.4 Models with PCM only

In order to be able to integrate a resulting effective thermal conductivity of the investigation into a system model, it is necessary to reduce the complexity of the model. Therefore, in the following, the fins and the PCM are not modeled separately, but exclusively by the PCM, whose material properties are adjusted accordingly.

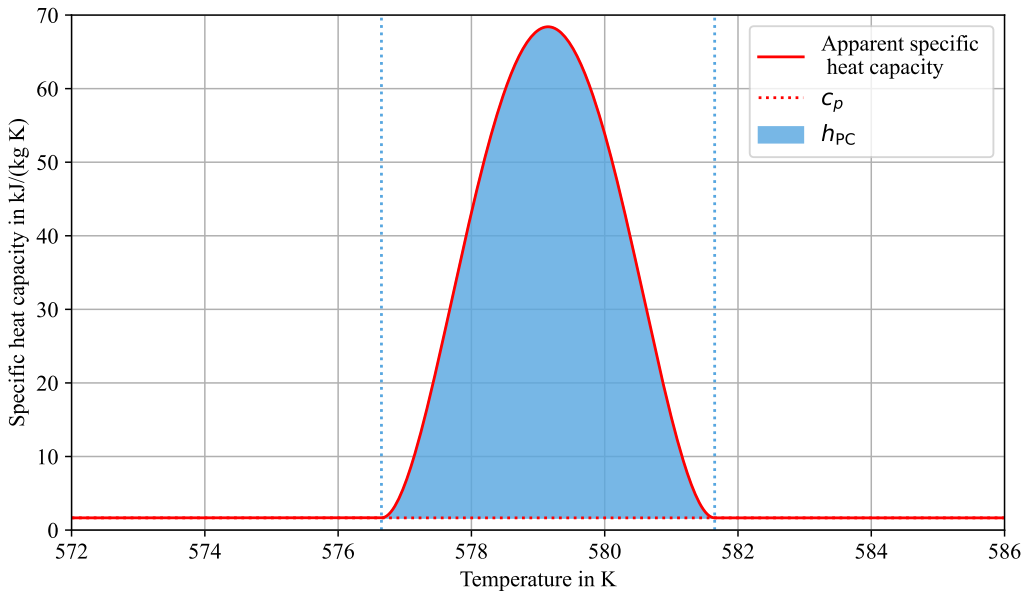


Figure 4: Distribution of the phase change enthalpy h_{PC} in the model with the apparent heat capacity method.
The blue dotted lines delimit the phase change interval

For the investigation of the effective thermal conductivity (Figure 3c), a constant temperature is set on the inside of the tube carrying the HTF, which would be present if the HTF were to condense or vaporize. An adiabatic boundary condition is defined on the outside. Symmetry boundary conditions are assumed both at the bottom and at the top.

The volume force and thus the natural convection are not modeled. Instead, only thermal conduction of the PCM is modeled. The aluminum fins are replaced by the PCM. To ensure comparability with the cases in which the fins are modeled, the density of the PCM is multiplied by the factor $\frac{l_{fin}}{l_{PCM}+l_{fin}}$ so that the heat capacity of the PCM remains unchanged, whereas that of the aluminum fins is omitted. This is justified by the fact that the aluminum fins are responsible for less than 2.5 % of the heat capacity of the fins and PCM in the case of the largest temperature interval passed through and thus at the greatest influence of the sensible amount of heat that can be stored in the fins.

To carry out a subsequent backtesting, the model described before is applied, whereby the values from the validation are used instead of the temperature specification and the losses are taken into account again, as can be seen in Figure 3d.

2.5 Evaluation of effective thermal conductivity

The aim of this study is to determine the most representative effective thermal conductivity for both the liquid and the solid phase. To determine these values, reference cases are first defined. In these cases, a temperature of 5 K, 10 K and 15 K above the melting temperature is applied to the inner wall of the tube for the charging process. For the subsequent discharging, temperatures are applied that are below the melting temperature by the same amounts. These temperatures are also specified as the initial temperatures.

The values presented are typical (5 K, 10 K) (Steinmann, 2022) or greater (15 K) than those for technical applications and therefore serve as the basis for the present study. The phase change temperature was used as the basis. The differences between the initial temperatures and the temperatures applied on the inner wall of the tube during charging are therefore twice the temperature differences mentioned.

In the model depicted in Figure 3c, all values between $10 \text{ W m}^{-1} \text{ K}^{-1}$ and $20 \text{ W m}^{-1} \text{ K}^{-1}$ are run through in steps of $1 \text{ W m}^{-1} \text{ K}^{-1}$ for both the liquid and the solid PCM applying the same temperatures as in the reference cases.

The root mean square error (RMSE) is used to determine the combinations that show the smallest deviations from the respective reference case for the temperatures and heat flows for the charging and discharging process. For the

calculation of the RMSE, the values of the first 15 min of charging and discharging are not taken into account in the case of the heat flows due to the strong spikes caused by high temperature gradients. In addition, the last 5 min of the charging process are excluded.

3 VALIDATION

The validation is based on experimental data taken from Laing et al., 2010. The reconstructed experimental data and the simulation results of the PCM temperature, which is calculated volumetrically averaged, is shown in Figure 5. As can be seen from the figure, a grid study was carried out. Four structured rectangular grids with a number of 855 (very coarse), 3277 (coarse), 12 600 (medium) and 49 500 grid elements (fine) were examined. The coarse grid proved to be sufficiently precise and was therefore used for further investigations.

The transition between the phase change process, which is accompanied by a flat temperature increase, and the further temperature increase of the PCM due to the absorption of sensible heat is more evident in the simulation than in the experiment. One of the reasons for this may be that only a section of the storage tank is considered in the model, whereas in the experiment the PCM may have reached different stages of melting along the direction of flow of the HTF. In the experiment, the average temperature can therefore rise as a result of the temperature increase of the PCM in parts of the LTES unit, while other parts of the LTES unit are still undergoing a phase change.

Furthermore, there are measurement uncertainties in the experiment that can affect both the average PCM temperature and the HTF temperatures. The latter were used for the validation case and backtesting, which means that deviations here can also affect the model.

Based on the above explanations, the model is therefore considered validated.

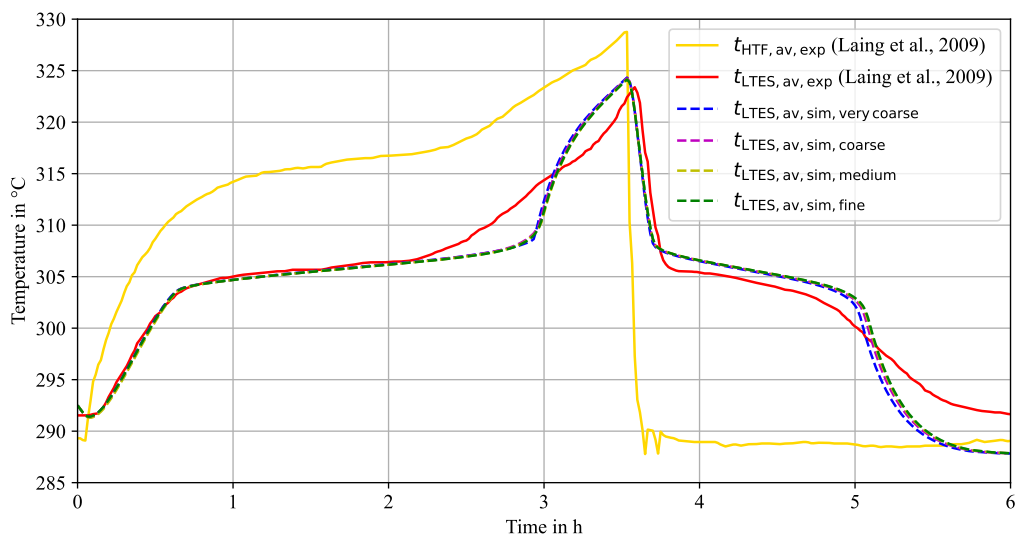


Figure 5: Experimental and simulation results of the average LTES unit temperature

4 RESULTS AND DISCUSSION

In this chapter, the results of the effective thermal conductivity investigation and the backtesting are presented. Afterward, a comparison is made with the literature.

4.1 Effective thermal conductivity investigation

For the investigation of the effective thermal conductivity, 3 h of charging and 3 h of discharging are specified. The results of the reference cases and the corresponding combinations of the effective thermal conductivities of the liquid and solid PCM with the lowest RMSE with respect to the average temperature are shown in Figure 6.

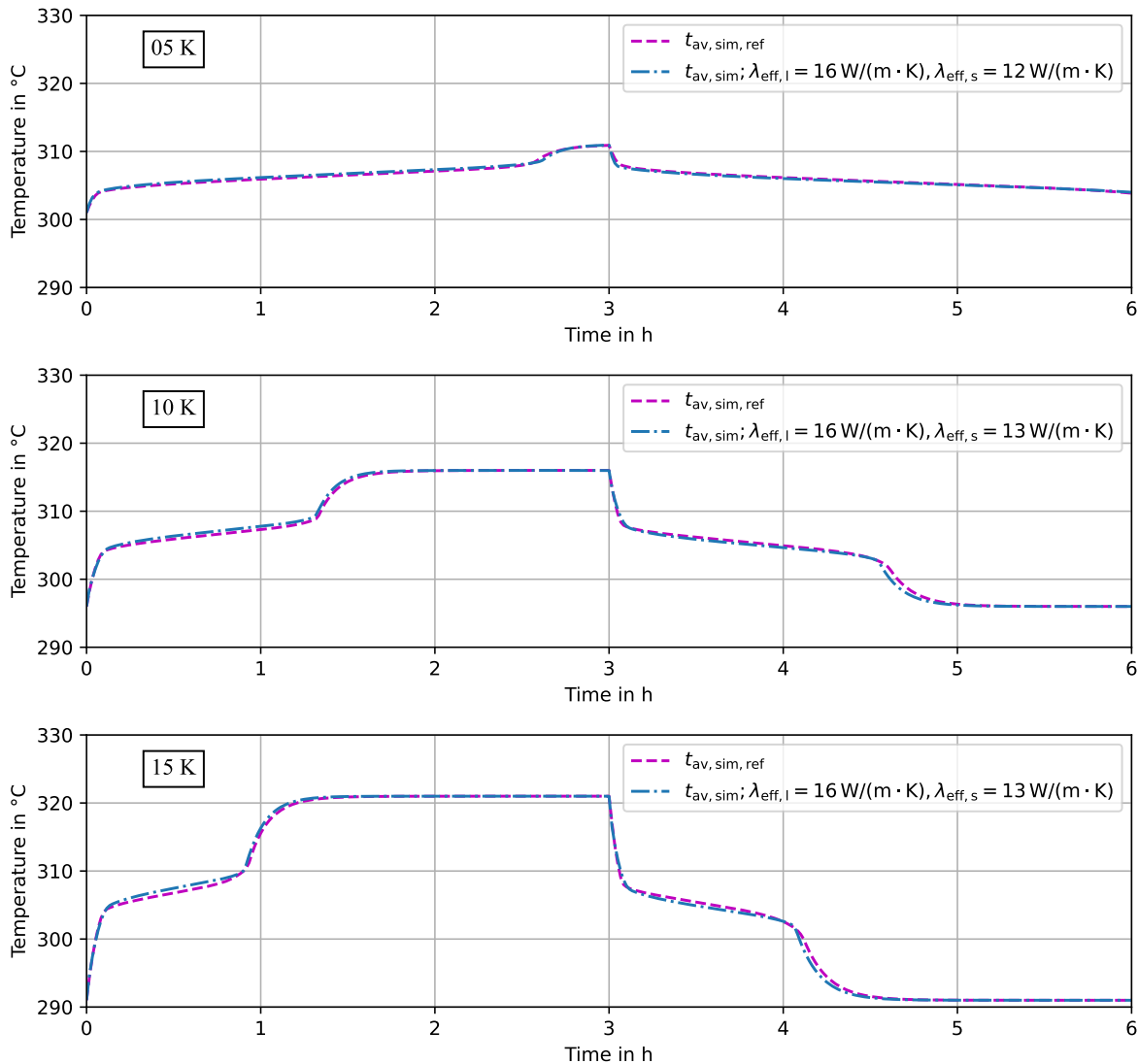


Figure 6: Average temperatures of the reference simulations and simulations with the lowest RMSE. From top to bottom: temperature difference between inner tube wall and melting temperature: 5 K, 10 K, 15 K.

The other 120 combinations resulting from the variation of the effective thermal conductivities are not shown for reasons of clarity. For a temperature difference of 5 K, it can be seen that the temperature specified on the inner wall of the tube has not yet been reached, both in the charging process and especially in the discharging process. Figure 7 shows the results of the reference cases and the combinations that have the lowest RMSE in terms of heat flow on the inner wall of the tube. For clarity, the additional 120 combinations are again not shown and the visible range of the heat flows is reduced to -20 W to 20 W . Thus, the spikes in heat flow at the beginning of the charging and discharging process are not shown completely in the figure. In accordance with the temperature curve at the temperature difference of 5 K in Figure 6, it can also be recognized from the heat flow that the discharging process in particular was not yet complete, as the heat flow has not yet reached zero.

The agreement between the simulation results with the simplified model and those with the corresponding reference cases is higher for the average temperatures than for the heat flows on the inner wall of the tube. The latter show higher deviations, especially at higher temperature differences (bottom of Figure 7).

It can be seen that the effective thermal conductivities with the highest agreement for both cases and all three investigated temperature differences show almost exclusively identical values. Only for the average temperature at a temperature difference of 5 K (top of Figure 6) the results based on the effective thermal conductivities $\lambda_{eff, l} = 16 \text{ W m}^{-1} \text{ K}^{-1}$ and $\lambda_{eff, s} = 12 \text{ W m}^{-1} \text{ K}^{-1}$ show the highest agreement. In all other cases, the results using effective thermal conductivities $\lambda_{eff, l} = 16 \text{ W m}^{-1} \text{ K}^{-1}$ and $\lambda_{eff, s} = 13 \text{ W m}^{-1} \text{ K}^{-1}$ are associated with the smallest

deviations from the reference cases. It is noticeable that the case in which the charging and discharging process was not fully completed in the simulation time is the deviating case.

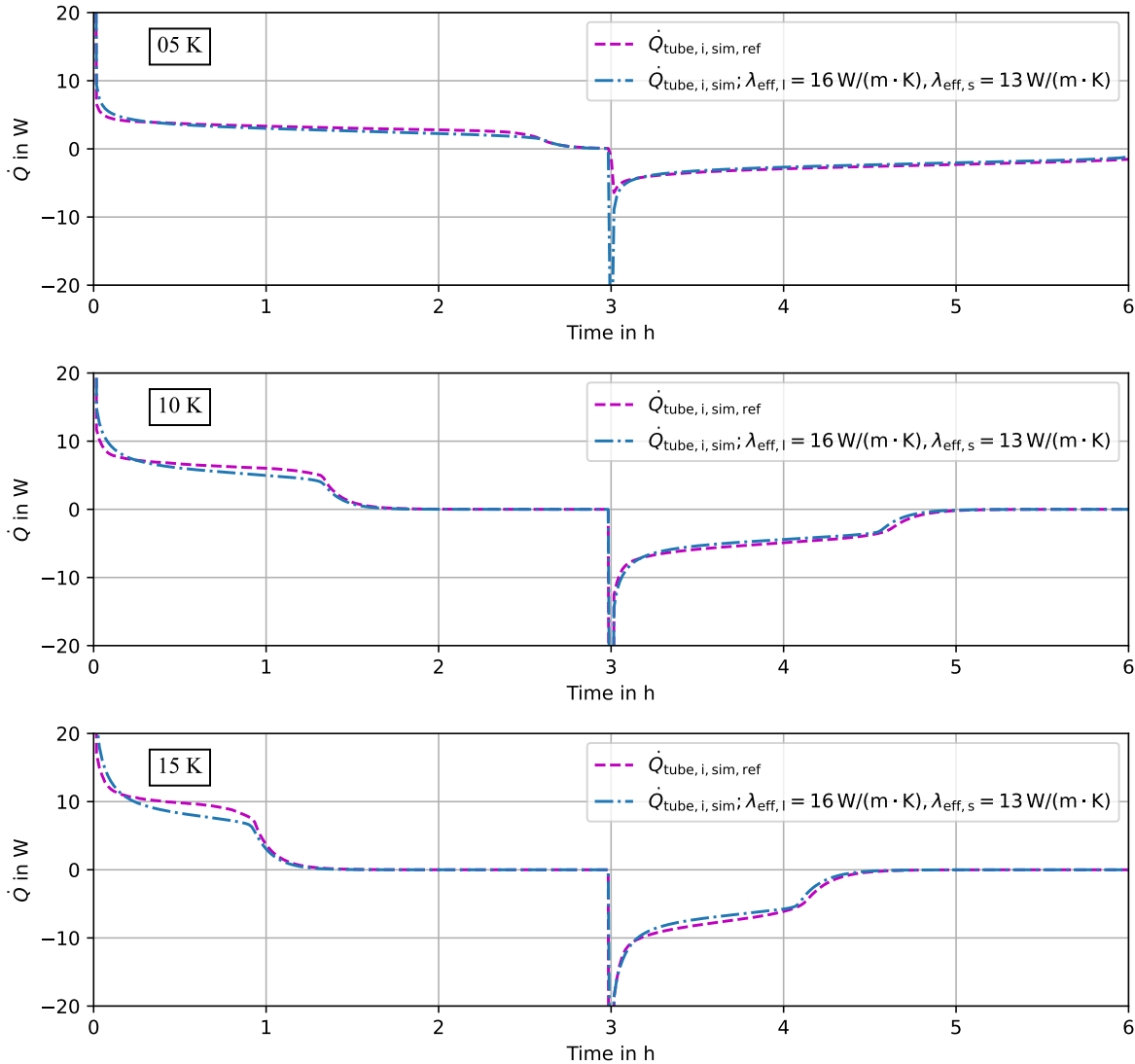


Figure 7: Heat flows on the inner wall of the tube to the modeled representative section of the reference simulations and simulations with the lowest RMSE. From top to bottom: temperature difference between inner tube wall and melting temperature: 5 K, 10 K, 15 K

4.2 Backtesting

In order to investigate the applicability of the effective thermal conductivities obtained to the validation case, backtesting is carried out. The model from Figure 3d is used for this, assuming an effective thermal conductivity of $16 \text{ W m}^{-1} \text{ K}^{-1}$ for the liquid PCM and $13 \text{ W m}^{-1} \text{ K}^{-1}$ for the solid PCM based on the results.

Figure 8 illustrates the outcomes. In addition to the measured values and the described case, the validation case with the coarse grid is shown to ensure direct comparability. In the charging process, the average temperature starts to rise earlier in the simulation that only includes the PCM. In addition, a higher maximum average temperature is reached. The average temperature also drops earlier during the discharging process and ends at approximately the same temperature as it ends with the validated model.

It is clear that the reduction of the model complexity leads to an increase in the deviation between the simulated and the measured average temperature of the LTES. Nevertheless, it can be stated that the model provides an adequate representation of the measured values in order to use the modeling approach in a system model. This can be concluded especially against the background that even the more complex model shows recognizable deviations

from the experimental data.

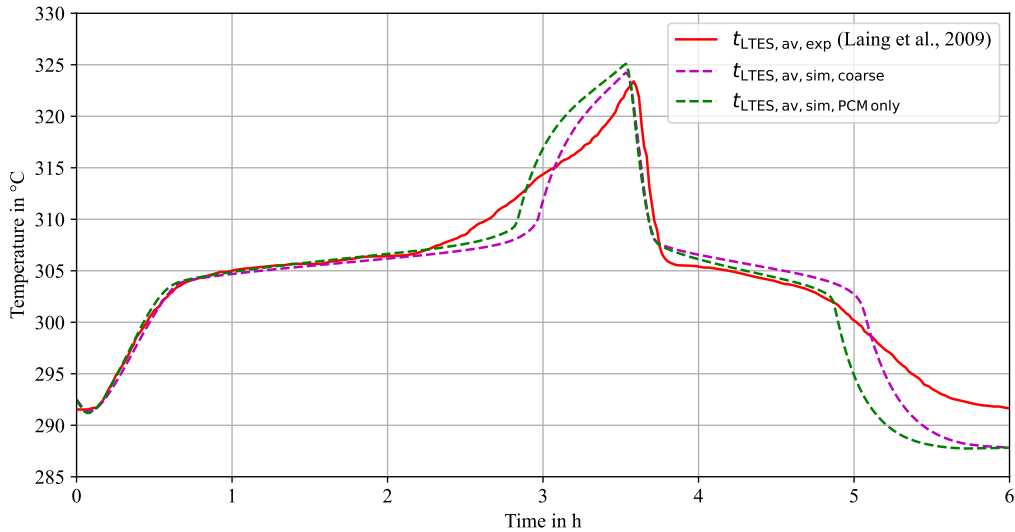


Figure 8: Experimental, validation simulation and backtesting simulation results of the average LTES unit temperature

4.3 Comparison to literature

Assuming a completely parallel arrangement of fins and PCM, the resulting effective thermal conductivities for the given configuration and the existing material values would be $21.56 \text{ W m}^{-1} \text{ K}^{-1}$ and $21.69 \text{ W m}^{-1} \text{ K}^{-1}$ for the liquid and solid phases of the PCM, respectively. A value of $0.55 \text{ W m}^{-1} \text{ K}^{-1}$ (Dietrich, 2017) is assumed for the thermal conductivity of the liquid PCM. According to the study by Vogel et al., 2020, which assumes a factor of 0.8 for the weighting of the parallel arrangement, this would result in values of $17.37 \text{ W m}^{-1} \text{ K}^{-1}$ and $17.51 \text{ W m}^{-1} \text{ K}^{-1}$ for the effective thermal conductivities mentioned. Compared to these two studies, the present investigation suggests lower effective thermal conductivities. The comparison with the weighting factor of Dietrich, 2017, which would result in effective thermal conductivities of $10.03 \text{ W m}^{-1} \text{ K}^{-1}$ and $10.19 \text{ W m}^{-1} \text{ K}^{-1}$, shows that the effective thermal conductivities in the present study are higher. The effective thermal conductivities determined in this study correspond to weighting factors of approximately 0.735 and 0.585 for the liquid and solid phases respectively.

5 CONCLUSION

This paper presents a simplified model of an LTES unit with hexagonal fins, modeled as annular fins. By replacing the structure of fins and PCM with the PCM only, it is possible to significantly reduce the model complexity. By comparing simulations that consider effective thermal conductivity for both the liquid and the solid PCM individually with simulations of a validated model that accounts for the exact geometry and natural convection, approximated values for the effective thermal conductivities could be determined. These are $16 \text{ W m}^{-1} \text{ K}^{-1}$ and $13 \text{ W m}^{-1} \text{ K}^{-1}$ for the liquid and solid PCM. The comparison of the simulation results with regard to the average LTES unit temperature shows that the simplified model has higher deviations. Nevertheless, the model can be considered sufficiently precise for use in system modeling.

In future studies, the procedure presented in this paper could be applied to configurations that are modified in terms of geometry or material. The influence of the varied parameters could be quantified in this way.

NOMENCLATURE

Abbreviations

HTF	Heat transfer fluid
LTES	Latent thermal energy storage
PCM	Phase change material
RMSE	Root mean square error

Symbols

c	specific heat capacity, $\text{J kg}^{-1} \text{K}^{-1}$
h	specific enthalpy, kJ kg^{-1}
l	length, mm
\dot{m}	mass flow rate, kg s^{-1}
\dot{Q}	heat flow, W
r	radius, mm
t	temperature, $^{\circ}\text{C}$
T	temperature, K
ΔT	temperature difference, K
v	velocity, m s^{-1}
α	heat transfer coefficient, $\text{W m}^{-2} \text{K}^{-1}$
β	coefficient of thermal expansion in K^{-1}
η	dynamic viscosity, $\text{kg m}^{-1} \text{s}^{-1}$
λ	thermal conductivity, $\text{W m}^{-1} \text{K}^{-1}$
ρ	density, kg m^{-3}

Superscripts and Subscripts

av	average
base	base value
char	charging
eff	effective
exp	experiment
fin	fin
l	liquid
loss	loss
NaNO_3	NaNO_3
o	outer
PC	phase change
ref	reference case
s	solid
sim	simulation
tube	tube

REFERENCES

Ali, H. M., Rehman, T.-u., Arıcı, M., Said, Z., Duraković, B., Mohammed, H. I., Kumar, R., Rathod, M. K., Buyukdagli, O., & Teggar, M. (2024). Advances in thermal energy storage: Fundamentals and applications. *Progress in Energy and Combustion Science*, 100, 101109.

Bauer, T., Laing, D., & Tamme, R. (2012). Characterization of sodium nitrate as phase change material. *International Journal of Thermophysics*, 33(1), 91–104.

COMSOL AB (Ed.). (2024). Comsol documentation: V. 6.2. Retrieved January 15, 2025, from <https://doc.comsol.com/6.2/docserver/#!/com.comsol.help.comsol/helpdesk/helpdesk.html>

Dietrich, A. (2017). Assessment of pumped heat electricity storage systems through exergoeconomic analyses.

Eastman Chemical Company (Ed.). (2022). Therminol® vp-1 heat transfer fluid: Ultrahigh-temperature, vapor/liquid phase fluid. Retrieved February 12, 2025, from <https://www.eastman.com/content/dam/>

eastman/corporate/en/literature/t/tf9141.pdf#:~:text=Eastman%20Therminol%C2%AE%20VP-1%20heat%20transfer%20fluid%20is%20specifically,optimum%20use%20range.%20Therminol%20VP-1%20is%20available%20globally.

Gnielinski, V. (2019). G1 wärmeübertragung bei erzwungener konvektion: Durchströmte rohre. In P. Stephan, S. Kabelac, M. Kind, D. Mewes, K. Schaber, & T. Wetzel (Eds.), *Vdi-wärmeatlas* (pp. 803–811). Springer Berlin Heidelberg.

Janz, G. J. (1967). *Molten salts handbook*. Academic Press. <https://ebookcentral.proquest.com/lib/kxp/detail.action?docID=1164591>

Jriri, T., Rogez, J., Bergman, C., & Mathieu, J. C. (1995). Thermodynamic study of the condensed phases of nano₃, kno₃ and csno₃ and their transitions. *Thermochimica Acta*, 266, 147–161.

Kirincic, M., Trp, A., Lenic, K., & Batista, J. (2024). Latent thermal energy storage performance enhancement through optimization of geometry parameters. *Applied Energy*, 365, 123255.

Laing, D., Bauer, T., Lehmann, D., & Bahl, C. (2010). Development of a thermal energy storage system for parabolic trough power plants with direct steam generation. *Journal of Solar Energy Engineering*, 132(2).

Laing, D., Bauer, T., Steinmann, W.-D., & Lehmann, D. (2009). Advanced high temperature latent heat storage system - design and test results. In *Effstock 2009*.

Nagasaki, Y., & Nagashima, A. (1991). The thermal conductivity of molten nano₃ and kno₃. *International Journal of Thermophysics*, 12(5), 769–781.

Nunes, V. M. B., Lourenço, M. J. V., Santos, F. J. V., & de Castro, C. A. N. (2006). Viscosity of molten sodium nitrate. *International Journal of Thermophysics*, 27(6), 1638–1649.

Parry, A. J., Eames, P. C., & Agyenim, F. B. (2014). Modeling of thermal energy storage shell-and-tube heat exchanger. *Heat Transfer Engineering*, 35(1), 1–14. <https://doi.org/10.1080/01457632.2013.810057>

Rohatgi, A. (2023). Webplotdigitizer. Retrieved June 14, 2024, from <https://apps.automeris.io/wpd4/>

Román, F., Munir, Z., & Hensel, O. (2024). Mathematical modelling of a latent heat storage: Influence of pcm thermal conductivity and enthalpy-temperature relationship. *Journal of Energy Storage*, 94, 112424.

Steinmann, W. D. (2022). *Thermal energy storage for medium and high temperatures: Concepts and applications*. Springer Fachmedien Wiesbaden GmbH.

Tay, N., Belusko, M., Castell, A., Cabeza, L. F., & Bruno, F. (2014). An effectiveness-ntu technique for characterising a finned tubes pcm system using a cfd model. *Applied Energy*, 131, 377–385.

Tehrani, S. S. M., Taylor, R. A., Saberi, P., & Diarce, G. (2016). Design and feasibility of high temperature shell and tube latent heat thermal energy storage system for solar thermal power plants. *Renewable Energy*, 96, 120–136. <https://doi.org/10.1016/j.renene.2016.04.036>

Tiari, S., & Hockins, A. (2021). An experimental study on the effect of annular and radial fins on thermal performance of a latent heat thermal energy storage unit. *Journal of Energy Storage*, 44, 103541.

Tiari, S., Hockins, A., & Mahdavi, M. (2021). Numerical study of a latent heat thermal energy storage system enhanced by varying fin configurations. *Case Studies in Thermal Engineering*, 25, 100999.

Ullrich, C., & Bodmer, T. (2019). D6.1 thermophysikalische stoffwerte von metallen und metalllegierungen. In P. Stephan, S. Kabelac, M. Kind, D. Mewes, K. Schaber, & T. Wetzel (Eds.), *Vdi-wärmeatlas* (pp. 645–658). Springer Berlin Heidelberg.

van der Hoeven, M. (2014). Technology roadmap: Energy storage (Organisation for Economic Co-operation and Development & International Energy Agency, Eds.).

Vogel, J., & Johnson, M. (2019). Natural convection during melting in vertical finned tube latent thermal energy storage systems. *Applied Energy*, 246, 38–52.

Vogel, J., Keller, M., & Johnson, M. (2020). Numerical modeling of large-scale finned tube latent thermal energy storage systems. *Journal of Energy Storage*, 29, 101389.

Waser, R., Ghani, F., Maranda, S., O'Donovan, T. S., Schuetz, P., Zaglio, M., & Worlitschek, J. (2018). Fast and experimentally validated model of a latent thermal energy storage device for system level simulations. *Applied Energy*, 231, 116–126. <https://doi.org/10.1016/j.apenergy.2018.09.061>

ACKNOWLEDGEMENT

Funding by the German Research Foundation within the Priority Program 2403: ‘Carnot-Batteries: Inverse Design from Markets to Molecules’ under project number 525974553 is gratefully acknowledged.

Thanks are also expressed to two Masters students, Arthur Rudek and Dominik Hering, whose work served as the basis for the development of the models presented in this study.